Implications on cosmology from Dirac neutrino magnetic moments

E. Grohs[1,2] and A. B. Balantekin[3]

[1]*Department of Physics, University of California Berkeley, Berkeley, California 94720, USA*
[2]*Department of Physics, North Carolina State University, Raleigh, North Carolina 27607, USA*
[3]*Department of Physics, University of Wisconsin-Madison, Madison, Wisconsin 53706, USA*

(Received 16 March 2023; accepted 17 May 2023; published 2 June 2023)

The mechanism for generating neutrino masses remains a puzzle in particle physics. If neutrino masses follow from a Dirac mass term, then neutrino states exist with opposite chirality compared to their weakly interacting counterparts. These inactive states do not interact with their active counterparts at measurable scales in the Standard Model. However, the existence of these states can have implications for cosmology as they contribute to the radiation energy density at early times, and the matter energy density at late times. How Dirac neutrinos may populate thermal states via an anomalous magnetic moment operator is the focus of this work. A class of models where all neutrinos have a magnetic moment independent of flavor or chirality is considered. Subsequently, the cross sections for neutrinos scattering on background plasma particles are calculated so that the relic inactive neutrino energy is derived as a function of plasma temperature. To do so, one needs cross sections for scattering on all electrically charged Standard Model particles. Therefore, the scattering cross section between a neutrino and W boson via the magnetic moment vertex is derived. Current measurements put a constraint on the size of the neutrino magnetic moment from the cosmological parameter N_{eff} and light-element primordial abundances. Finally, how the extra Dirac states contribute to the matter energy density at late times is investigated by examining neutrino free streaming.

DOI: 10.1103/PhysRevD.107.123502

I. INTRODUCTION

In his "Dear Radioactive Ladies and Gentlemen" letter to the Tübingen meeting of the German Physical Society (reproduced in Ref. [1]) Wolfgang Pauli, in addition to proposing the existence of neutrino itself, implied that the neutrino is massive and hence it interacts via its magnetic dipole moment. Since Pauli did not explore the possibility of a new kind of interaction, i.e., the weak interaction, the magnetic moment he could deduce was too large. After the weak interaction was introduced by Enrico Fermi and it was realized that neutrinos could be massless, interest in the electromagnetic interactions of neutrinos waned since symmetry considerations suggest that neutrino magnetic moment would vanish for massless neutrinos. Earlier surveys did not come up with any experimental evidence for electromagnetic interactions of neutrinos [2]. However, as solar neutrino experiments found increasingly strong evidence for the presence of nonzero neutrino masses, papers exploring astrophysical and cosmological implications of a nonzero neutrino magnetic moment started to appear in the literature [3–11]. Indeed one of the solutions of the solar neutrino problem was to invoke interactions of neutrinos with solar magnetic fields [12].

Within the Standard Model, neutrinos are taken to be massless. If indeed neutrinos are massive, as the solar neutrino experiments suggested, then the question arise as to how they obtain their masses in an extension to the Standard Model. Since they are neutral fermions, a neutrino mass term added to the Standard Model Lagrangian can produce a discernible difference between Dirac or Majorana character. A Dirac neutrino is distinct from its antiparticle: Dirac neutrinos carry lepton number $+1$ and Dirac antineutrinos carry lepton number -1. Conversely, a Majorana neutrino is identical to its antiparticle and consequently there is no conserved lepton number with Majorana neutrinos. A free Dirac neutrino, like all the other charged fermions, is described by a spinor with four independent components. In contrast, since a Majorana neutrino is its own antiparticle (i.e., equal to its charge-conjugate up to a phase), its spinor has only two independent components. A direct consequence of this is that a Majorana neutrino cannot have a diagonal (i.e., connecting two mass eigenstates that are the same) magnetic moment, but magnetic moments connecting two different mass eigenstates are permitted. Dirac neutrinos have no such constraint.

Published by the American Physical Society under the terms of the Creative Commons Attribution 4.0 International license. Further distribution of this work must maintain attribution to the author(s) and the published article's title, journal citation, and DOI. Funded by SCOAP[3].

Determining the Dirac versus Majorana character of neutrinos is a major area of research and there exist many terrestrial experiments dedicated to this search, e.g., neutrinoless double beta decay [13–20]. Complementary to the terrestrial searches, there has been a long history of using cosmology to probe neutrino properties and interactions. Early work by Schramm and his collaborators [21,22] connecting the number of neutrinos to cosmological parameters and observables brought those efforts to the forefront. This work particularly emphasized using the effective relativistic degrees of freedom, $N_{\rm eff}$, and the neutrino mass density in the Universe to constrain the neutrino parameters. The interplay of terrestrial experiments and cosmological observations continues to the present day [23] and this work follows in the same spirit.

Only left-handed neutrinos (and right-handed antineutrinos),[1] which are referred to as "active," take place in weak interactions. Any neutral fermion that does not participate in weak interactions is "sterile," although this term is more frequently used for those neutral fermions that mix with the active states and have different mass eigenvalues. To avoid confusion in this work, we will label the opposite chirality Dirac states (right-handed neutrinos and left-handed antineutrinos) as "inactive." Additional interactions of neutrinos beyond the weak interactions (such as electromagnetic couplings) allow neutrinos to remain in thermal contact longer during the big bang nucleosythesis (BBN) epoch [3]. Imposing the condition that production of inactive neutrino states does not alter the primordial ^{4}He abundance Morgan obtained a limit of $\sim 10^{-11}\mu_B$ [4] on the neutrino magnetic moment, where $\mu_B = e/(2m_e)$ is the Bohr magneton. Further imposing the condition that inactive states do not increase the effective relativistic degrees of freedom in excess of one more neutrino species, Morgan's limit was relaxed by a factor of ~ 3 [24]. This limit only applies to Dirac neutrinos since for Majorana neutrinos right-handed states are not additional neutrino states but represent antineutrinos. The energy dependence of the reaction cross sections due to the contribution of the electromagnetic couplings of neutrinos is different than that of the usual weak interaction couplings. For Majorana neutrinos with transition (i.e., connecting two different mass eigenstates) magnetic moments such reactions convert neutrinos into antineutrinos and vice versa. The resulting change in the reaction rates would alter the way neutrinos decouple from the plasma of electrons/positrons and photons. Such considerations can be used to limit magnetic moments of Majorana neutrinos as was done in Ref. [25]. The purpose of this paper is to improve limits on the magnetic moments of Dirac neutrinos using a careful assessment of the physics of decoupling in the early Universe, i.e., the epoch at which the scattering rates of inactive neutrinos become too small to maintain thermal equilibrium with the plasma of Standard Model constituents.

To determine the decoupling of the inactive neutrinos, we require a form for the electromagnetic interaction. We introduce the electromagnetic vertex function to characterize electromagnetic interactions below electroweak symmetry breaking [26]

$$F_\alpha(k) = f_Q(k^2)\gamma_\alpha + f_M(k^2) i\sigma_{\alpha\beta}k^\beta - f_E(k^2)\sigma_{\alpha\beta}k^\beta\gamma_5 + f_A(k^2)(k^2\gamma_\alpha - k_\alpha \not{k})\gamma_5. \quad (1)$$

In Eq. (1), we adopt the conventions $\sigma_{\alpha\beta} = i[\gamma_\alpha, \gamma_\beta]/2$, $\gamma_5 = -i\gamma^0\gamma^1\gamma^2\gamma^3$, and $\not{k} = \gamma_\alpha k^\alpha$. f_Q, f_M, f_E, and f_A are the electric monopole, magnetic dipole, electric dipole, and anapole form factors, respectively, for momentum transfer k_α. Using the operator for the magnetic dipole interaction in Eq. (1), we will calculate scattering amplitudes, cross sections, and rates as a function of plasma temperature T. We calculate both elastic scattering ($\nu + c \leftrightarrow c + \nu$) and annihilation ($\nu + \bar{\nu} \leftrightarrow c + \bar{c}$) processes between neutrinos and charged particles c. As a result of considering the scattering interactions at times after the electroweak transition (EWT), we take the Higgs and electroweak bosons as massive particles. A corollary of this treatment is the inclusion of electromagnetic interactions between $W^\pm$ bosons and neutrinos, which we will show have profound effects on setting limits on the neutrino magnetic moment. We will loosen the restriction for the quark-hadron transition (QHT)—where quark and gluon degrees of freedom disappear and are replaced by hadrons—and consider epochs before and after this transition. The QHT is included using the approximate treatment described in Appendix C and based off of Ref. [27].

The outline of this paper is as follows. We summarize neutrino magnetic moment interactions and the pertinent cosmology in Secs. II and III, respectively. Our results for the early and later Universe are given in Secs. IV and V. In Sec. VI we present our conclusions. Appendices A and B cover description of differential cross sections with magnetic moment vertices and thermal averaging of the cross sections. Appendix C details our treatment of the QHT. Throughout this work, we use natural units where $\hbar = c = k_B = 1$.

II. MAGNETIC MOMENTS

Comprehensive reviews of neutrino electromagnetic interactions in the context of both the Standard Model and physics beyond the Standard Model are available in the literature [28–30]. The value of the neutrino magnetic moment in the minimally extended (i.e., to include the neutrino mass) standard electroweak theory is very small.

[1]We note that these states should properly be called left chiral or right chiral, not left handed or right handed. Nevertheless, we adopt the nomenclature present in the literature when referring to the chiral states.

Using the expression for the one-loop electromagnetic vertex for fermions [31] it was calculated to be order of $10^{-20}\mu_B$ [32]. Given our current knowledge of the neutrino masses and mixing angles, the updated prediction of the Standard Model, minimally extended to allow massive neutrinos, for the electron neutrino magnetic moment is even smaller [33]. In contrast, the most stringent laboratory limit on the neutrino magnetic moment obtained from electron scattering experiments is orders of magnitude larger: $2.9 \times 10^{-11}\mu_B$ [34]. Recently excess electron recoil events at the XENON1T detector [35] was interpreted as a possible signature of the neutrino magnetic moment [36]. PandaX collaboration reports a neutrino magnetic moment limit of $4.9 \times 10^{-11}\mu_B$ using the low energy electron recoil events [37]. A recent analysis of the LUX-ZEPLIN data similarly limits the effective neutrino magnetic moment data to be less than $1.1 \times 10^{-11}\mu_B$ [38]. Finally, a recent analysis of XENONnT data yields the most stringent limit for electron-flavor neutrino magnetic moment of $0.9 \times 10^{-11}\mu_B$ [39]. All three limits would rule out the neutrino magnetic moment interpretation of the XENON1T data.

Large magnetic moments of neutrinos would have very interesting implications for astrophysics and cosmology. If there is an electromagnetic channel to produce neutrinos besides the usual weak one, then these additional neutrinos transfer more of the energy and entropy over large distances. It was remarked quite some time ago that extra energy loss due to the additional electromagnetic neutrino pair emission can limit the value of neutrino magnetic moment [2]. Indeed right after the observation of SN 1987A, it was shown that bounds on the flux of right-handed neutrinos from a core-collapse supernova can be translated into bounds on neutrino magnetic moments [40–42]. Perhaps the tightest astrophysical bound comes from red giant stars at globular clusters; the increased energy loss resulting from the electromagnetic neutrino pair production near the helium flash could lead to an increased core mass [7]. The most recent such analysis yields a limit in the range of $(1.2 - 1.5) \times 10^{-12}\mu_B$ [43]. Other energy loss arguments typically yield less stringent limits. For example additional energy losses would eliminate the blue loops in the evolution of intermediate-mass stars; hence for Cepheid stars to exist, the neutrino magnetic moment should be smaller than the range $\sim 2 \times 10^{-10}\mu_B - 4 \times 10^{-11}\mu_B$ [44]. Similarly if the neutrino magnetic moment is of the order of $10^{-12}\mu_B$, additional energy losses can explain the enhanced lithium abundance observed in red clump stars [45]. An examination of the pulsations [46] or the luminosity function of hot white dwarfs [47] give similar limits. However such limits are subject to large uncertainties, such as the rate of the ^{12}C reaction or the stellar metallicity. It was suggested that it is possible to evade such astrophysical limits [48] by invoking new interactions of the neutrino with a light scalar boson [49–51]. One can use spin-flavor precession of neutrinos to assess the value of the neutrino magnetic moment. A more recent analysis using this approach with ultra-high-energy neutrinos is consistent with a limit of $1.2 \times 10^{-11}\mu_B$ [52]. More recent work from astrophysics and cosmology considered transition magnetic moments between active and additional sterile neutrino states [53–55]. These limits are also of the order of $10^{-11}\mu_B$.

The constraints on neutrino magnetic moment, such as those listed in the previous paragraph, are obtained considering neutrino electromagnetic scattering takes place in a plasma consisting of charged particles and antiparticles in the early Universe. In such an environment screening of photons needs to be taken into account. We adopt a static screening prescription. Hence photons acquire an effective mass, which we denote by m_γ. The inverse of this mass is the Debye screening length for electromagnetic interactions. It is given by

$$m_\gamma^2 = \frac{1}{\lambda_D^2} = 4\pi\alpha \sum_i q_i^2 \frac{\partial}{\partial \mu_i}\left[n_i^{(-)} - n_i^{(+)}\right]. \tag{2}$$

In Eq. (2), α is the fine structure constant, $n_i^{(\mp)}$ is the number density for particles (antiparticles), respectively. The partial derivative is with respect to the particle chemical potential and q_i is the charge coefficient of the particle for each particle-antiparticle pair (e.g., for an electron-positron plasma $q_i^2 = 1$). Assuming thermal equilibrium and vanishing chemical potentials and masses for all particles, we obtain

$$m_\gamma^2|_{m_i=0,\mu_i=0} = \frac{2\pi\alpha}{3} T^2 \sum_i q_i^2 g_i, \tag{3}$$

where T is the plasma temperature and g_i are the internal degrees of freedom from spin, color, etc. The effective photon mass is plotted in Fig. 1 as a function of the

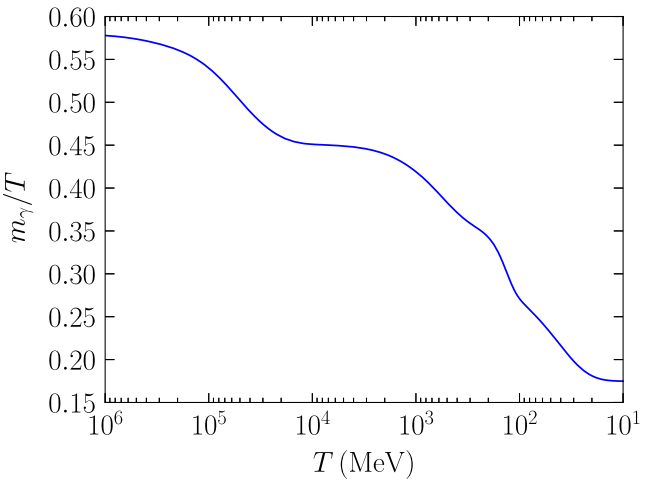

FIG. 1. Effective in-medium photon mass plotted as a function of plasma temperature [see Eq. (2)].

temperature. At very early times many particles are present in the plasma. As the Universe evolves, the particle-antiparticle pairs annihilate one by one into lighter particles and no longer contributing to the effective photon mass in Eq. (2).

One can also explore dynamic effects on neutrinos coming from the plasma background [56,57] The authors of Refs. [58,59] explored such effects and found changes in $N_{\rm eff}$ comparable to what we describe later in this article. This is perhaps not unexpected. For example in Ref. [60] it was reported that light element abundances in BBN does not change when one considers dynamic screening.

In our analysis we will use only the magnetic-moment term of the neutrino electromagnetic vertex function in Eq. (1), namely $f_M(k^2)i\sigma_{\alpha\beta}k^\beta$. We adopt the symbol κ for the neutrino magnetic moment, defined as the magnetic dipole form factor in the forward-scattering limit, i.e., $\kappa \equiv f_M(k^2=0)$, which we scale to the Bohr magneton as

$$\kappa = \mu \frac{e}{2m_e}, \tag{4}$$

using the dimensionless parameter μ and not to be confused with the chemical potentials in Eq. (2). We will include the effective photon mass from Eq. (2) when calculating scattering amplitudes and the resultant cross sections and rates. For example: including in-medium effects modifies the well-known differential cross section expression for elastic scattering from charged fermions to the following

$$\left(\frac{d\sigma}{dt}\right)_{\nu f} = \frac{\pi q_f^2 \alpha^2}{m_e^2}\mu^2 \frac{t}{(t-m_\gamma^2)^2}\frac{s+t-m_f^2}{s-m_f^2} \tag{5}$$

for each charged fermion with a mass m_f and charge coefficient q_f. In Eq. (5), the magnetic moment μ is given in units of Bohr magneton, hence m_e in the prefactor is the same for all fermions since it comes from the definition of μ_B. s and t are the usual Mandelstam variables.

We list the differential cross sections used in this work in Appendix A. To obtain integrated cross sections, these expressions need to be integrated from $t_{\rm min} = -(s-m_i^2)^2/s$ to $t_{\rm max} = 0$ to give the cross section as a function of s and T, for each target mass m_i. Returning to the example for the differential cross section in Eq. (5), integrating over t gives

$$\sigma_{\nu f}(s) = \frac{\pi q_f^2\alpha^2}{m_e^2}\mu^2\left[\left(1+\frac{2m_\gamma^2}{s-m_f^2}\right)\log\left(1+\frac{(s-m_f^2)^2}{sm_\gamma^2}\right) - \frac{s-m_f^2}{s} - 1 + \frac{m_\gamma^2 m_f^2}{sm_\gamma^2+(s-m_f^2)^2}\right]. \tag{6}$$

We have explicitly given the cross section for elastic scattering off of fermions in Eq. (6), but for all the other cross sections we numerically integrate the differential cross sections. After obtaining a cross section like the one in Eq. (6), we can calculate the thermal average of cross section multiplied by the Moller speed [61], namely

$$\langle \sigma_k v_{\rm Mol}\rangle = \frac{\frac{g_1 g_2}{(2\pi)^6}\int d^3p_1 \frac{1}{e^{E_1/T}+1}\int d^3p_2 \sigma_k v_{\rm Mol}\frac{1}{e^{E_2/T}\pm 1}}{\frac{g_1 g_2}{(2\pi)^6}\int d^3p_1 \frac{1}{e^{E_1/T}+1}\int d^3p_2 \frac{1}{e^{E_2/T}\pm 1}}, \tag{7}$$

where the k subscript indicates a specific scattering target and process. In writing Eq. (7), we have assumed equilibrium distributions for the incoming neutrino (labeled as particle 1) and the scattering target (particle 2) and ignored the Pauli blocking/Bose enhancement of the products. The ± 1 in the distribution function for particle 2 corresponds to either fermions (+) or bosons (−). For elastic scattering, the target particle is charged, whereas for annihilation it is an antineutrino. Appendix B gives simplified expressions for Eq. (7) in the case of scattering off of either fermions or bosons, and the annihilation process.

The last step in the procedure is to calculate the scattering rate using the thermally averaged $\langle \sigma_k v_{\rm Mol}\rangle$ number density of incoming neutrinos, n_ν

$$\Gamma_k = n_\nu \langle \sigma_k v_{\rm Mol}\rangle. \tag{8}$$

Including the example specifically given in Eq. (5), we calculate the individual rates for the processes of elastic scattering and annihilation for each charged particle target or product. Summing over all of the individual rates gives us a total scattering rate Γ_ν as a function solely of temperature and μ.

Returning again to the example in Eq. (6), one can see that to leading order σ does not scale with temperature. In fact, $\langle \sigma v_{\rm Mol}\rangle$ also does not scale with T to leading order. Only the number density n_ν in Eq. (8) provides a nontrivial T^3 scaling. The Hubble expansion rate scales as T^2, implying that the magnetic moment interaction keeps the inactive neutrino states thermally populated at high temperatures, but become ineffective at lower temperatures.

III. COSMOLOGY

The scattering and annihilation rates via the magnetic-moment vertex all scale as μ^2, implying that increasing μ will increase the interaction rate and postpone the point when the inactive states decouple from the plasma. In principle, decoupling could occur at low temperatures when the matter energy density comprises a significant fraction of the total energy density. As we will show in Sec. IV, current cosmological bounds imply that inactive neutrinos must decouple at early times, when the Universe is dominated by radiation.

For radiation-dominated conditions, we will parametrize the energy density in two different ways. When doing a calculation to determine decoupling, we use the parameter $g_\star$ as an effective spin statistic constant [62]

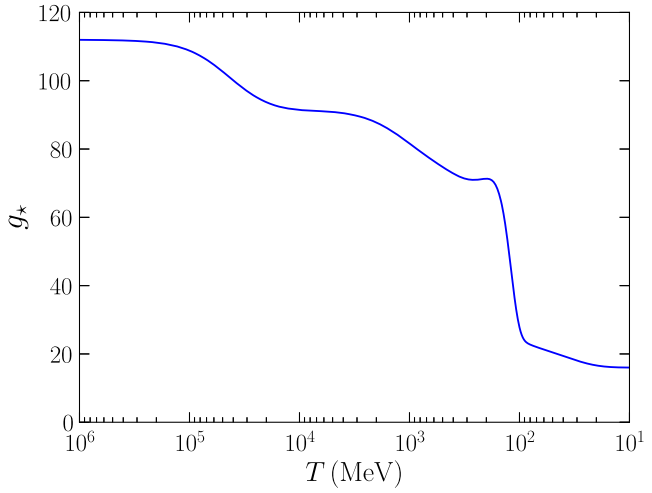

FIG. 2. Hubble expansion rate parameter $g_\star$ plotted as a function of temperature. Included in the calculation of $g_\star$ are the six degrees of freedom from the inactive neutrino states.

$$\rho = \frac{\pi^2}{30} g_\star T^4. \tag{9}$$

When showing results on extra radiation energy density, we use the effective number of degrees of freedom, $N_{\rm eff}$, to parametrize the radiation energy density. We delay discussion of $N_{\rm eff}$ until Sec. IV. $g_\star$ contains contributions from massless and massive particles. To determine $g_\star$, we first calculate the total energy density using the appropriate Bose-Einstein or Fermi-Dirac (FD) equilibrium distribution function

$$\rho = \sum_i g_i \int \frac{d^3p}{(2\pi)^3} E f_i(E), \tag{10}$$

where the energy E is related to the rest mass m_i through $E = \sqrt{p^2 + m_i^2}$. We equate Eqs. (9) and (10) and solve for $g_\star$ as a function of temperature. Figure 2 shows the relation between $g_\star$ and plasma temperature employed in our decoupling calculations. At the TeV scale, the entire Standard Model is present with ultrarelativistic kinematics. As the Universe expands and the temperature decreases, the equilibrium abundances of massive particles become Boltzmann suppressed and their respective degrees of freedom vanish. The "plateau-hill" pattern in Fig. 2 shows multiple instances of vanishing degrees of freedom. When the temperature reaches 10 MeV, only photons, electrons, and neutrinos contribute to $g_\star$. Included in the calculation of $g_\star$ are the six inactive neutrino states at all temperatures.

To construct the plot in Fig. 2 we make a number of simplifying assumptions. First, we take the masses of the Higgs, vector bosons, and the top quark to be constant and equal to their vacuum values at all times. In reality, these and other particles acquire their masses during the EWT which occurs at ∼140 GeV [63]. As a result, our values for $g_\star$ for $T \sim 140$ GeV are an underestimate in Fig. 2. Second, we use a fitting function to model the dynamics of the QHT centered at $T \sim 170$ MeV. The fitting procedure produces a local maximum at $T \sim 200$ MeV when bound hadronic states coexist with free quarks and gluons. Despite the local maximum, the energy density monotonically decreases with decreasing temperature at all times during the transition. Appendix C gives details on the fitting procedure adopted from Ref. [27].

Equation (9) ignores any contribution to the total energy density from matter or vacuum, appropriate for our purposes of inactive neutrino decoupling in the radiation-dominated regime. We can calculate the Hubble expansion rate with $g_\star$ to yield

$$H = \sqrt{\frac{8\pi}{3m_{\rm pl}^2}\rho} = \sqrt{\frac{4\pi^3}{45} g_\star}\frac{T^2}{m_{\rm pl}}, \tag{11}$$

where $m_{\rm pl} = 1.2 \times 10^{19}$ GeV is the Planck mass. Equation (11) shows that the Hubble expansion rate scales as T^2. The previous section showed that the magnetic-moment interaction rates scale as $\sim T^3$. As a result, inactive neutrinos will maintain thermal equilibrium with the plasma at high temperatures, and eventually freeze-out and free stream at lower temperatures. Figure 3 shows the total magnetic-moment interaction rate (solid blue) and Hubble expansion rate (dashed green) each as a function of temperature. For this particular example, the magnetic-moment strength is taken to be $\mu = 10^{-13}$. For our purposes, we approximate decoupling as an instantaneous event when the interaction rate falls below the Hubble expansion rate

$$\Gamma_\nu < H \Rightarrow \text{decoupled}. \tag{12}$$

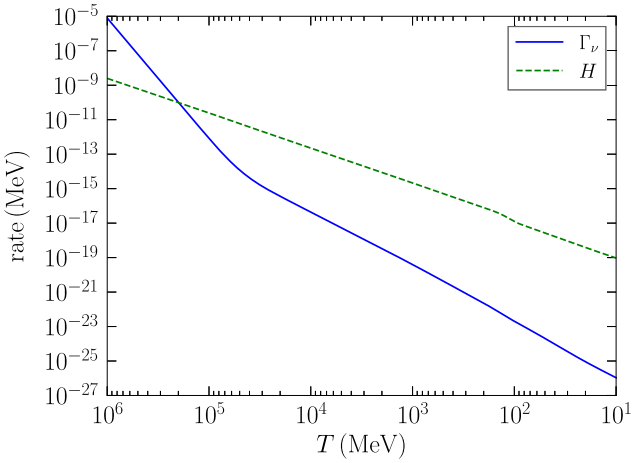

FIG. 3. Rates plotted against temperature. The inactive neutrino scattering rate (solid blue) is for a magnetic moment strength $\mu = 10^{-13}$. Also given is the Hubble expansion rate (dashed green).

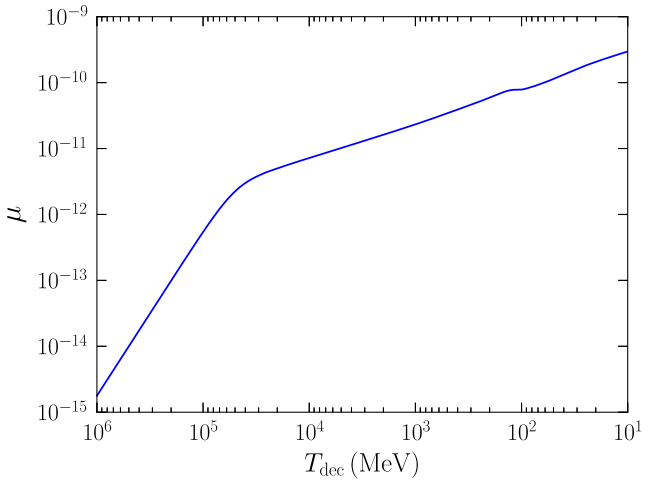

FIG. 4. Magnetic moment strength μ, corresponding to an interaction rate below the Hubble expansion rate, plotted as a function of decoupling temperature.

For the example in Fig. 3 we estimate the decoupling temperature as $T_{\rm dec} \simeq 200$ GeV. The magnetic-moment interaction rate scales as T^3 at low temperatures. Once $W^{\pm}$ bosons are present in the plasma ($T \sim 100$ GeV), the interaction rate increases dramatically, scaling as T^7. This change in the scaling law is present in Fig. 3 at a temperature scale comparable to the $W^{\pm}$ rest mass.

In our calculations, the magnetic-moment interaction rate is solely a function of the dynamical variable T and the model parameter μ. All interaction rates are proportional to μ^2, so an individual rate has the same temperature dependence as the blue curve in Fig. 3 with an overall scaling dependent on μ. As a result, we can fix a decoupling temperature $T_{\rm dec}$ and solve for the corresponding μ by locating where the interaction rate falls below the Hubble expansion rate. Figure 4 shows the magnetic moment strength as a function of the decoupling temperature. The general behavior of the curve shows that increasing magnetic-moment strengths delays decoupling. The shoulder at $T \sim 100$ GeV is again due to the presence of $W^{\pm}$ bosons in the plasma, akin to the behavior of the blue curve in Fig. 3.

IV. EARLY UNIVERSE RESULTS

With the presence of the inactive Dirac states, there exists more energy density in the neutrino sector. The inactive states have identical mass eigenvalues to those of the active neutrinos, and so their masses are small. At early times, before photon decoupling, all of the neutrinos are ultrarelativistic and their energy density contributes to radiation. At later times and the current epoch, the neutrino energy density contributes to matter. In this section we discuss the implications at early times for the cosmic microwave background (CMB) and BBN.

During atomic recombination, the radiation energy density is composed of photons, active neutrinos, and inactive neutrinos. We assume that inactive-neutrino decoupling and active neutrino decoupling preserve the Fermi-Dirac spectra of the various neutrino species (see Refs. [64–72] among others on noninstantaneous decoupling). The implication is that we can use temperaturelike variables for the three components of the radiation. Therefore, we write the radiation energy density during recombination as the following:

$$\rho_{\rm rad} = \frac{\pi^2}{15} T^4 + 3 \times \frac{7\pi^2}{120} T_a^4 + 3 \times \frac{7\pi^2}{120} T_i^4, \tag{13}$$

where T_a is the active neutrino temperaturelike quantity, and T_i is a comparable quantity for the inactive neutrinos. Conservation of comoving entropy gives the familiar relation between T_a and T [62]

$$\frac{T_a}{T} = \left(\frac{4}{11}\right)^{1/3}. \tag{14}$$

The same principle applies for deducing the ratio T_i/T, and we find

$$\frac{T_i}{T} = \left(\frac{43}{11}\frac{1}{g_{\star,S}^{\rm dec}}\right)^{1/3}, \tag{15}$$

where $g_{\star,S}^{\rm dec}$ is the effective entropic degrees of freedom at inactive-neutrino decoupling $T_{\rm dec}$ (see Fig. 4). $g_{\star,S}^{\rm dec}$ is related to $g_{\star}^{\rm dec}$ by subtracting off the inactive neutrino degrees of freedom

$$g_{\star,S}^{\rm dec} = g_{\star}^{\rm dec} - \frac{7}{8} \times 6. \tag{16}$$

Using the cosmological parameter $N_{\rm eff}$ and the temperature ratios in Eq. (13), we can relate $N_{\rm eff}$ to $g_{\star,S}^{\rm dec}$

$$N_{\rm eff} = 3\left[1 + \left(\frac{43}{11}\frac{1}{g_{\star,S}^{\rm dec}}\right)^{4/3}\right]. \tag{17}$$

Figure 5 shows the change in $N_{\rm eff}$ in the presence of the inactive neutrino states. The vertical axes are the change in $N_{\rm eff}$ from 3, namely

$$\Delta N_{\rm eff} \equiv N_{\rm eff} - 3 = 3\left(\frac{43}{11}\frac{1}{g_{\star,S}^{\rm dec}}\right)^{4/3}. \tag{18}$$

The horizontal axes give a range of μ. In the top panel, we show the entire range of μ studied in this work, where the lower limit corresponds to $T_{\rm dec} \sim 1$ TeV and the upper limit to $T_{\rm dec} \sim 1$ MeV. For the large magnetic-moment strengths, the inactive neutrinos decouple at the same time

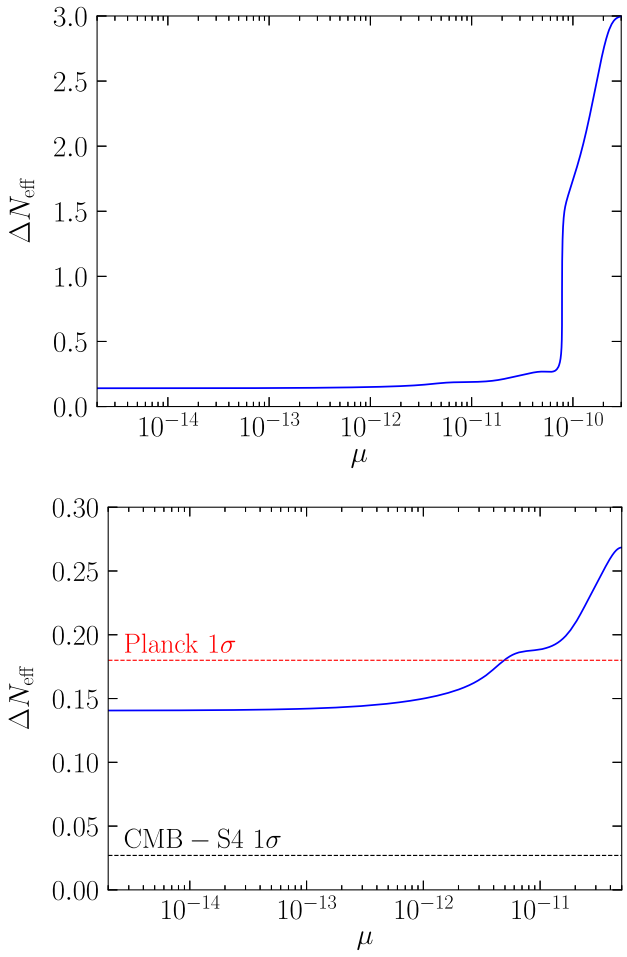

FIG. 5. Change in $N_{\rm eff}$ versus magnetic moment strength. The top panel shows the entire range of magnetic moments explored in this work. The bottom panel is a narrow range for low values of μ. Also plotted is the 1σ uncertainty from the Planck mission [73] and the proposed 1σ uncertainty from CMB-S4 [74].

as the active neutrinos do, implying that $T_a = T_i$ and both sectors contribute equally to $N_{\rm eff}$.

The bottom panel of Fig. 5 shows a restricted range of μ, corresponding to decoupling before the QHT. We have inserted horizontal lines to show the 1σ limits from the *Planck* mission [73] and projections from CMB Stage IV [74]. We observe that at the level of 1σ, $\mu \simeq 5 \times 10^{-12}$ would produce a value of $N_{\rm eff}$ in tension with *Planck*. In the future, if CMB-S4 does not see any evidence of extra radiation energy density, then Dirac neutrinos could not have been in thermal equilibrium below the EWT to nearly 4σ level.

With an increase in radiation energy density, the Hubble expansion rate also increases which leads to an earlier epoch of weak freeze-out and nuclear freeze-out during BBN [75] (see Ref. [76] for the present status on BBN observations). Figure 6 shows the relative differences in the helium-4 mass fraction, $Y_{\rm P}$, and the ratio of deuterium to hydrogen, D/H, as solid blue and dashed green lines,

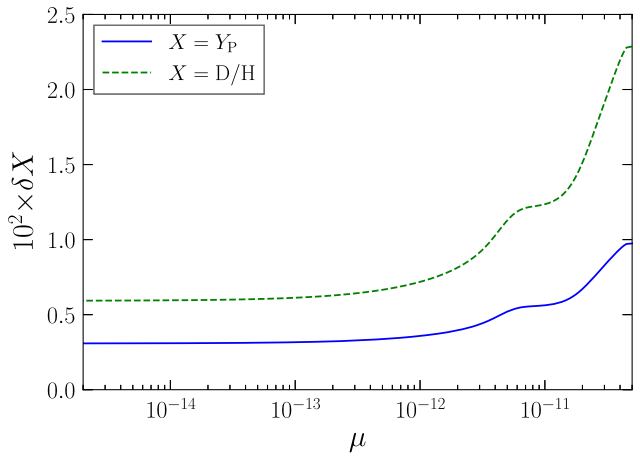

FIG. 6. Relative changes in primordial abundances plotted as a function of μ. The solid blue curve gives the relative change in the helium mass fraction $(Y_{\rm P})$ and the dashed green curve gives the relative change in the deuterium abundance (D/H).

respectively. The relative differences are computed by comparing to a baseline where there are no inactive Dirac states, and the active neutrinos decouple at a temperature of 10 MeV. The horizontal axis in Fig. 6 is the same range in μ as the bottom panel of Fig. 5. The shapes of the curves in Fig. 6 and $\Delta N_{\rm eff}$ in Fig. 5 are all similar to one another as the abundances linearly scale with $N_{\rm eff}$ in this range [77]. D/H is more sensitive to $N_{\rm eff}$ and so has a larger deviation from the baseline value than $Y_{\rm P}$. For $\delta({\rm D/H}) < 1\%$, $\mu \lesssim 4 \times 10^{-12}$, in line with the 1σ Planck limit from Fig. 5.

V. LATER UNIVERSE RESULTS

For the various epochs prior to photon decoupling, neutrino masses are small compared to the momenta, and so we approximated neutrinos as massless for calculations of energy density and interaction rates in Sec. IV. After neutrinos decouple from electrons and positrons (an epoch well before the photon-decoupling one), they continue to have ultrarelativistic kinematics and move at speeds nearly that of light. During these later epochs neutrino kinematics will become increasingly nonrelativistic in an expanding Universe. Accordingly, neutrino 3-momenta will redshift and asymptotically approach zero, implying the neutrino rest mass contribution evolves from a negligible to the dominant component of the neutrino energy density. As a result, we will need to discard our early Universe approximation of neutrinos being massless.

Typically, the dynamics of massive neutrinos is included in cosmology by extending the ΛCDM model to include the "sum of the light neutrino masses" parameter, denoted as Σm_ν [78,79]. The presence of neutrino rest mass changes the growth of smaller versus larger-scale structure as neutrinos free stream during the initial stages of structure formation, but act as component of the total matter energy

density at later stages. The difference in the structure growth rates yields a modified matter power spectrum, which can be elucidated by considering weak gravitational-lensing of the CMB convolved with matter distributions from cosmological surveys [80]. The transition between the small and large-scale regimes depends on Σm_ν, but also depends on the spectrum of the neutrinos. If we introduce a nonthermal portion to the total cosmic neutrino spectrum via a low-energy contribution from the inactive Dirac states, we change the epoch when neutrinos become nonrelativistic and hence the matter power spectrum and weak-lensing potential are appropriately altered.

A theoretical calculation of the lensing potential in the presence of anomalous magnetic moments for massive neutrinos is beyond the scope of our exploratory work. As an alternative to calculating the lensing potential, we will investigate the dependence of Σm_ν and μ on free streaming. Neutrinos move at speeds less than the speed of light, implying the more massive the neutrino the earlier it will become nonrelativistic over the history of the Universe. This implies a smaller free-streaming scale, $\lambda_{\rm fs}$. We will use the free-streaming wave number $k_{\rm fs} = 2\pi a/\lambda_{\rm fs}$ (at scale factor a) to evaluate the roles of neutrino rest mass and anomalous magnetic moment strength on late-time cosmology.

Neutrinos will begin to move at speeds appreciably less than the speed of light once their momenta become comparable to their masses. The results of $N_{\rm eff}$ from the previous section showed that the inactive neutrinos must decouple from the plasma prior to the active neutrinos, implying that the comoving temperature quantity for the inactive states, T_i, is smaller than the counterpart quantity for the actives, T_a. In fact, if $T_i \ll T_a$, there is a possibility that the inactive states could become nonrelativistic in the early Universe. For the range of magnetic moment strength we consider in this work, the inactive states do not become nonrelativistic until well after photon decoupling.

We adopt the definition of $k_{\rm fs}$ from Eq. (93) in Ref. [78]

$$k_{\rm fs}(t) = \sqrt{\frac{3}{2}}\frac{a(t)H(t)}{v_{\rm th}(t)}, \tag{19}$$

where t is the time coordinate and $v_{\rm th}$ is akin to the thermal speed with more explanation below. For our purposes, we will use the scale factor a as an independent variable. If we consider the current epoch where $a = a_0$, we will denote the free-streaming wave number as $k_{\rm fs,0}$. To incorporate the physics of anomalous magnetic moments, we will calculate the thermal speed using an ensemble average over the inactive and active states. We describe both the active and inactive neutrino states using FD distributions with their respective comoving temperature quantities. All mass eigenstates for the active neutrinos have the same distribution with T_a, and similarly for the inactive states with T_i. Due to $T_i \neq T_a$, the thermal speed is not a true thermal average, but instead an ensemble average. Nevertheless, we adopt the nomenclature of thermal speed for consistency with the literature. The thermal speed in our cosmology with anomalous magnetic moments is

$$v_{\rm th} = \frac{2\times\sum_{j=1}^{3}\int_0^\infty \frac{d^3p}{(2\pi)^3}\frac{1}{e^{p/T_a}+1}\frac{p}{E_j} + 2\times\sum_{j=1}^{3}\int_0^\infty \frac{d^3p}{(2\pi)^3}\frac{1}{e^{p/T_i}+1}\frac{p}{E_j}}{2\times\sum_{j=1}^{3}\int_0^\infty \frac{d^3p}{(2\pi)^3}\frac{1}{e^{p/T_a}+1} + 2\times\sum_{j=1}^{3}\int_0^\infty \frac{d^3p}{(2\pi)^3}\frac{1}{e^{p/T_i}+1}}, \tag{20}$$

where $E_j = \sqrt{p^2 + m_j^2}$ and the summations over j are for the three separate mass eigenstates. Note that T_i and T_a redshift with scale factor, so $v_{\rm th}$ also depends on scale factor. At high temperatures—equivalently low scale factor a—the neutrinos are ultrarelativistic and $p/E \sim 1$ and so $v_{\rm th} \sim 1$. Conversely, at high scale factor $p/E < 1$. We can simplify Eq. (20) to the following:

$$v_{\rm th} = \frac{2}{9\zeta(3)[T_a^3 + T_i^3]}\int_0^\infty d\epsilon \frac{\epsilon^2}{e^\epsilon + 1}\sum_{j=1}^{3}\left[\frac{T_a^3}{\sqrt{1+(\frac{m_j}{\epsilon T_a})^2}} + \frac{T_i^3}{\sqrt{1+(\frac{m_j}{\epsilon T_i})^2}}\right], \tag{21}$$

where we have used $\epsilon = p/T_x$ for either $x = a, i$. Figure 7 shows the evolution of $k_{\rm fs}$ as a function of the ratio a/a_0. To plot $k_{\rm fs}$, we need the following model input parameters: the ratios of temperature quantities T_i/T and T_a/T; and the light neutrino mass eigenstates. T_i/T is a function of the magnetic moment strength μ implied in Eq. (15), and $T_a/T = (4/11)^{1/3}$. For the mass eigenstates, we use the parameter Σm_ν and specify an ordering, either normal or inverted, using the solar and atmospheric mass splitting values where appropriate [81]. For both curves in Fig. 7, we pick $\mu = 1.88\times10^{-14}$. The solid blue curve uses $\Sigma m_\nu = 60.6$ meV with a normal mass ordering, i.e., a smallest mass eigenvalue $m_1 = 1$ meV. To show the effect of mass on $k_{\rm fs}$, we also plot a dashed green curve using massless neutrinos, i.e., using $v_{\rm th} = 1$. The neutrino energy density differs between the two cosmologies. For the purposes of

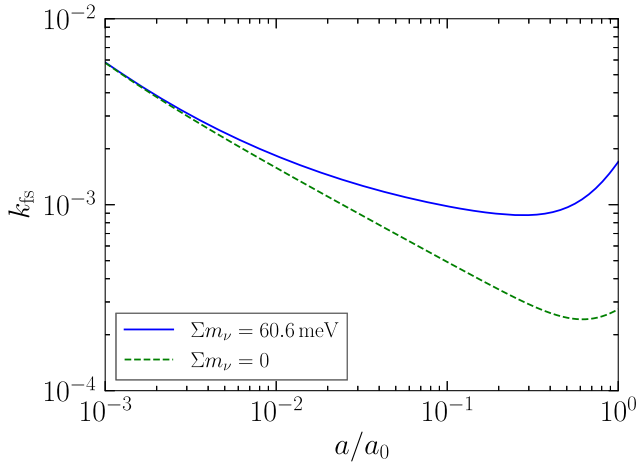

FIG. 7. $k_{\rm fs}$ plotted as a function of expansion parameter ratio a/a_0. Solid blue line is for massive neutrinos as given in Eq. (21) with $\Sigma m_\nu = 60.6$ meV in the normal mass ordering. Dashed green line is $k_{\rm fs}$ if neutrinos were massless, i.e., $m_j = 0$ in Eq. (21). For both curves, we take the neutrino magnetic moment strength to be $\mu = 1.88 \times 10^{-14}$.

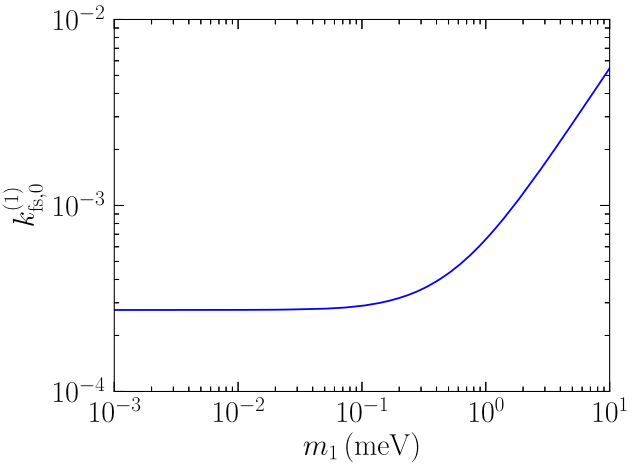

FIG. 8. Free-streaming wave number for the neutrinos with lightest mass eigenvalue m_1 plotted as a function of m_1 (meV). $k^{(1)}_{\rm fs,0}$ is calculated by setting the summations in Eq. (20) for $v_{\rm th}$ only to range over $j = 1$, and includes active and inactive neutrinos for the model $\mu = 1.88 \times 10^{-14}$.

comparing the two models, we preserve the Hubble expansion rate at the current epoch by adjusting the vacuum energy density, i.e., we decrease ρ_Λ for increasing Σm_ν. For $a/a_0 \gtrsim 10^{-3}$, we see that the blue curve diverges from the green curve due to massive neutrinos becoming nonrelativistic. The increase in $k_{\rm fs}$ corresponds to a decrease in power on small scales at later times. The divergence increases to the current epoch, at which point $k_{\rm fs}$ differs by an order of magnitude between the two cosmologies. For concreteness, we give the two values at the current epoch

$$k_{\rm fs,0}(\Sigma m_\nu = 60.6\ \text{meV}) = 1.70 \times 10^{-3}, \tag{22}$$

$$k_{\rm fs,0}(\Sigma m_\nu = 0\ \text{meV}) = 2.74 \times 10^{-4}. \tag{23}$$

We have employed a cosmology in Fig. 7 where the magnetic-moment interaction populates the inactive states resulting in a larger value of $N_{\rm eff}$. At this point, we give a brief digression to discuss how neutrino rest mass affects $k_{\rm fs}$ when magnetic moments are not present but $\Delta N_{\rm eff} > 0$. For a cosmology where $\Delta N_{\rm eff} = 0$, yet neutrinos have nonzero masses, we can compensate for the larger neutrino energy density by using a smaller vacuum energy density fraction, Ω_Λ, to preserve the Hubble expansion rate at the current epoch. We use the same prescription when $\Delta N_{\rm eff} > 0$, regardless of whether that extra radiation energy density is from neutrinos or some other undetermined particles. For the base values of Ω_Λ and the cold dark matter fraction we use in this work [73], a small decrease in Ω_Λ implies a younger Universe, and therefore a lower value of the free streaming length and larger value of $k_{\rm fs}$. When we introduce the inactive Dirac states via $\mu = 1.88 \times 10^{-14}$, $k_{\rm fs,0}$ does not vary at all from the base cosmology if neutrinos were massless. This is a result of $v_{\rm th} = 1$ and our prescription of fixing the Hubble expansion rate at the current epoch to be the same in Eq. (19) regardless of the cosmological model. On the other hand, for massive neutrinos with $\Sigma m_\nu = 60.6$ meV and $v_{\rm th} \neq 1$, the value in Eq. (22) is 5% higher than the comparable cosmological model with massive neutrinos and unpopulated inactive states.

Figure 7 shows the impact on $k_{\rm fs}$ when neutrinos become nonrelativistic. At the current epoch, the CMB photon temperature is $T = 2.726$ K, implying that the active neutrino temperature is $T_a = 0.17$ meV. For $\Sigma m_\nu = 60.6$ meV in a normal ordering, the neutrinos with the two heavier mass eigenvalues are nonrelativistic and have been for much of the history of the Universe. Decreasing Σm_ν below 60.6 meV to its absolute minimum of 59.6 meV only slightly changes the values of m_2 and m_3, but it has a significant effect on $k_{\rm fs}$. Although Σm_ν changes by less than 2%, $k_{\rm fs}$ decreases by nearly 60%. The decrease is entirely due to the kinematics of the neutrinos with the smallest mass eigenvalue m_1. Figure 8 shows the quantity $k^{(1)}_{\rm fs,0}$ plotted against m_1. $k^{(1)}_{\rm fs,0}$ is the free-streaming wave number for only the neutrinos with $m = m_1$. We calculate $k^{(1)}_{\rm fs,0}$ by first replacing the summations in Eq. (20) for $v_{\rm th}$ with single calculations where $m_j = m_1$, and then calculating the free-streaming wave number with Eq. (19). For $m_1 = 1$ meV, Fig. 8 shows that the distribution of lightest mass neutrinos is in transition from ultrarelativistic to nonrelativistic at the current epoch. Decreasing $m_1 \lesssim 0.1$ meV ensures the lightest neutrinos are ultrarelativistic for the entire history of the Universe.

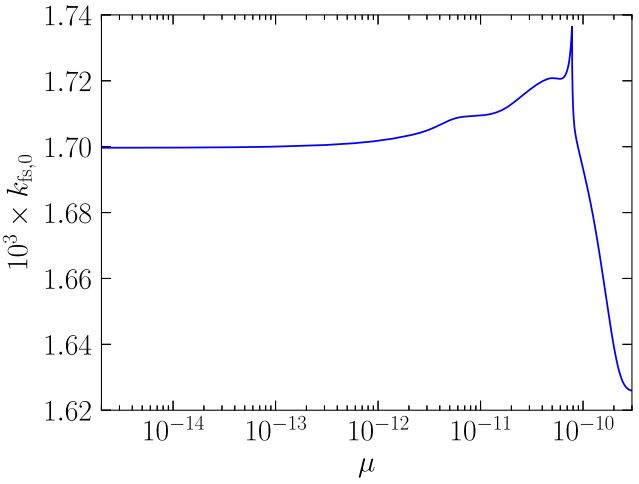

FIG. 9. $k_{\mathrm{fs},0}$ plotted as a function of magnetic moment strength μ. $\Sigma m_\nu = 60.6$ meV in the normal ordering.

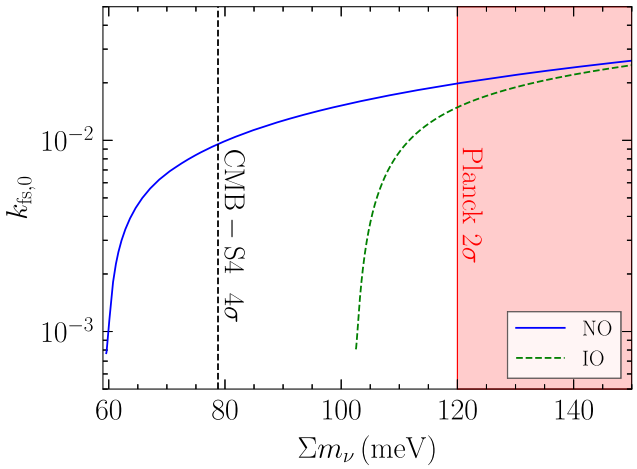

FIG. 10. $k_{\mathrm{fs},0}$ from Eq. (21) plotted as a function of Σm_ν (meV). Solid blue line is for the normal ordering, and dashed green line for the inverted ordering. Plot is for the model $\mu = 1.88 \times 10^{-14}$. Also plotted are the current constraints on Σm_ν from the Planck mission at 2σ (Ref. [73]) and a forecast from CMB-S4 at 4σ (Ref. [74]).

We have used a model where $\mu = 1.88 \times 10^{-14}$ when plotting $k^{(1)}_{\mathrm{fs},0}$ in Fig. 8. For other values of μ, $k^{(1)}_{\mathrm{fs},0}$ vs. m_1 would look qualitatively identical to Fig. 8. One of the quantitative differences for differing μ models is the value of m_1 where the kinematics of the neutrinos transition from relativistic $(E = \sqrt{p^2 + m^2})$ to ultrarelativistic $(E = p)$, represented by the ramp-up from the plateau of $k^{(1)}_{\mathrm{fs},0}$ in Fig. 8. There are two competing effects that alter the point of departure from the plateau. First, the inactive neutrino temperature is always smaller than the active neutrino temperature, and so the inactive neutrinos with a given mass depart from ultrarelativistic kinematics before the actives with that same mass in the history of the Universe. Figure 4 implies that the ratio T_i/T_a decreases with decreasing μ, so models with smaller μ have earlier points of departure in Fig. 8. However, in opposition to this first effect is the fact that smaller T_i implies a smaller number density for the inactive neutrinos. A smaller number density increases k_{fs} (and by extension $k^{(1)}_{\mathrm{fs},0}$) in Eq. (21), implying models with smaller μ would have a later point of departure in Fig. 8.

To show the competition between temperature and number density, we consider how $k_{\mathrm{fs},0}$ varies with μ for a fixed m_1 or equivalently a fixed Σm_ν. Figure 9 shows how $k_{\mathrm{fs},0}$ changes with μ for $\Sigma m_\nu = 60.6$ meV in a normal ordering. The higher values of μ show the effect of T_i/T_a close to unity, whereas the lower values show the effects of a smaller number density. There is a global maximum for these models at $\mu \lesssim 10^{-10}$, corresponding to a decoupling temperature $T_{\mathrm{dec}} \simeq 100$ MeV. This epoch occurs in proximity to the QHT and therefore the exact value of the global maximum is dependent on the treatment of the QHT. The shape of the curve in Fig. 9 is a function of the temperature ratio T_i/T_a. A larger value of Σm_ν acts to shift the curve down to smaller values of $k_{\mathrm{fs},0}$ while preserving T_i/T_a and the shape of that curve.

Finally, we show how $k_{\mathrm{fs},0}$ changes with Σm_ν for the normal (solid blue) and inverted (dashed green) orderings in Fig. 10. Both curves use a model where $\mu = 1.88 \times 10^{-14}$. The apparent asymptote at the lowest values of Σm_ν for each ordering are a result of neutrinos with mass eigenvalue m_1 staying ultrarelativistic until the current epoch, analogous to the descent to the plateau in Fig. 8. $k_{\mathrm{fs},0}$ has a smaller minimum value for the normal ordering as a result of a smaller neutrino energy density and older Universe. We have plotted the 2σ constraint on Σm_ν from the Planck mission [73] and a 4σ forecast from CMB-S4 [74]. If CMB-S4 finds a nonzero value for Σm_ν, then scales such as the free-streaming length would differ between the two orderings.

VI. CONCLUSIONS

The mechanism which generates the neutrino mass has yet to be determined, and as a result the nature of whether neutrinos are Majorana or Dirac is unknown. In this work, we have considered the cosmological implications on the existence of the inactive Dirac states and how they may be thermally populated at an early epoch in the history of the Universe. Both Dirac and Majorana neutrinos could impact N_{eff} through undetected interactions. For example, electromagnetic scattering of electrons and positrons with Majorana neutrinos changes the spectra of the active component through a heat flow from the electromagnetic plasma into the neutrino seas [25]. In the models considered in this work, electromagnetic scattering channels of charged particles with Dirac neutrinos populate the

TABLE I. Summary of limits on neutrino magnetic moments. Adapted from Table III of Ref. [86].

Method	Limit (in units of μ_B)	Notes
Reactor	2.9×10^{-11}	GEMMA [34]
Accelerator ν_e-e^-	10^{-11}	LAMPF [82]
Accelerator $(\nu_\mu, \bar{\nu}_\mu)$-e^-	6.8×10^{-10}	LSND [83]
Accelerator $(\nu_\tau, \bar{\nu}_\tau)$-$e^-$	3.9×10^{-7}	DONUT [84]
Dark matter direct detection	4.9×10^{-11}	PandaX [37]
Dark matter direct detection (ν_e)	0.9×10^{-11}	XENONnT [39]
Solar (^{7}Be)	5.4×10^{-11}	Borexino [85]
Red giant stars	1.2×10^{-12}	Ref. [43]
Cepheid stars	2×10^{-10}	Ref. [44]
Lithium in red clump stars	10^{-12}	Ref. [45]
Cosmology (Majorana)	10^{-10}	Ref. [25]
Cosmology (Dirac)	5×10^{-12}	This work ($N_{\rm eff}$ limit from Planck [73])

inactive states while preserving the FD spectra of the active states.

Motivated by the search for phenomenological differences between the Majorana versus Dirac nature of neutrinos, we studied a class of interactions between Dirac neutrinos and Standard Model particles not mediated by the weak force. As a hypothesis, the model we employed utilizes anomalous neutrino magnetic moments and an associated electromagnetic vertex, namely $i\kappa\sigma_{\alpha\beta}k^\beta$ in Eq. (1), to couple neutrinos to charged leptons, quarks, and $W^\pm$ bosons. We calculated thermally averaged cross sections for both the elastic scattering and the annihilation processes using the Debye screening length to reflect the bath of charged particles present in the plasma of the early Universe. In addition, we calculated the two scattering cross sections between neutrinos and $W^\pm$ for the first time using a magnetic moment vertex (see Appendix A). With these cross sections, we compare the associated scattering rates to the Hubble expansion rate to find a decoupling temperature as a function of the neutrino magnetic moment, parametrized using μ. Figure 4 shows the relation between the decoupling temperature and μ, where the scaling law changes around $T \sim 100$ GeV due to the presence of the $W^\pm$ bosons.

With the additional neutrino states populated, we were able to calculate changes to $N_{\rm eff}$, the primordial abundances $Y_{\rm P}$ and D/H, and the free-streaming wave number. Our strongest limits on μ come from those of $N_{\rm eff}$ using parameter estimations from the *Planck* mission [73]. Table I gives limits from experiments [34,82–85], other astrophysical or cosmological sources [25,43–45], and finally our current work, and will be further constrained with upcoming CMB experiments. More specifically, the relation between $N_{\rm eff}$ and μ in Fig. 5 is sensitive to how one treats the EWT and QHT. In terms of computing direct energy density, the QHT is obviously the more sensitive probe. However, if CMB-S4 pushes the limits on $N_{\rm eff}$ to epochs preceding the QHT, the EWT becomes more pertinent. We caution though that the EWT is not well understood and the scaling relations between the rates and μ may differ above electroweak symmetry breaking. Our results above ~ 100 GeV should be taken as extrapolations.

We note two points about our work which is unique to Dirac neutrinos but not anomalous magnetic moments in the context of cosmology. The first is the fact that there must exist three eigenstates for the inactive states with mass eigenvalues identical to the active neutrinos. When considering the energy density of a new low-mass particle in the early Universe, Dirac neutrinos come with a factor of 3 attached and as a result increase the energy density over that of a single neutral fermion [see both Fig. (21) in Ref. [74] and Ref. [87]]. Second and related to the first, the inactive neutrinos have nonzero masses—negligible at early times but not at late. Structure growth and neutrino free streaming are indeed dependent on the population of the inactive neutrinos, although those states cannot be thermally populated. A corollary of this result is that the inactive states must have different temperatures or spectra than the actives. Together, the low-mass and extra states of Dirac neutrinos give two methods to probe the neutrino spectra and search for new physics in cosmology.

We have examined the implications of Dirac neutrinos with anomalous magnetic moments on early and late-time cosmology in this work; and is a follow-up to the Majorana case of Ref. [25]. In a standard seesaw mechanism [30,88], the three active states are Majorana neutrinos; the three sterile states have mass eigenvalues much heavier than the active states and cannot be probed by current cosmological observations. However, there exists a possibility that those three sterile states could have mass eigenvalues nearly degenerate with the active ones. This possibility of neutrinos being "pseudo-Dirac" has been studied in the case of the diffuse supernova background [89] and mentioned in the case of early time cosmology [90]. If this mass model holds and neutrinos have anomalous magnetic moments, then they are Majorana particles and the analysis of BBN

in Ref. [25] would apply. In addition, the analyses on early and late time cosmological energy density in this work would also be relevant. Although such a hybrid situation is intriguing, Ref. [25] showed that the magnetic moment needs to be $\sim 10^{-10}\mu_B$ to influence the neutron-to-proton rates (and subsequent abundances) through altered neutrino spectra. If additional nonactive or sterile states can be populated via an anomalous magnetic moment, then Fig. 5 shows that the $N_{\rm eff}$ would be nearly 6.0 and ruled out by current cosmological parameter estimation. For early time cosmology, pseudo-Dirac cannot be distinguished from uniquely Dirac via anomalous magnetic moments.

Where there might be a difference between these two mass models is interpreting Σm_ν from large-scale-structure growth. If $\kappa < 10^{-10}\mu_B$ and the mass eigenvalues for the sterile states are nearly degenerate, then this situation is a close reproduction to the situation studied in Sec. V. To be precise, we would need to slightly alter the summations over the sterile states in Eq. (20) to account for different masses, although this should not make a significant difference if the sterile mass eigenvalues are nearly degenerate with the active ones. If, however, the sterile masses are smaller than the active ones, then there would be a contribution to $N_{\rm eff}$ but not to the dark-matter contribution at late times (see Fig. 8), thereby changing the free-streaming scale for the active neutrinos. In addition, lighter sterile states also introduce the possibility of active neutrino decays that alter the dynamics in late-time cosmology [91–93]. For this scenario of light sterile states and anomalous magnetic moments, pseudo-Dirac and uniquely Dirac give different predictions in late-time cosmology.

Finally, we comment on an often quoted result in the literature, colloquially referred to as the "Kayser confusion theorem" [94,95]. The theorem points out that other neutrino properties could lead to similar effects as the magnetic moment in scattering processes. Specifically, a Dirac magnetic moment could be confused with a Majorana anapole moment [see the f_M and f_A terms in Eq. (1)]. In this connection it is worthwhile to point out that cosmology differs from particle-beam experiments in one key aspect. In brief, the cosmological parameters $N_{\rm eff}$ and Σm_ν give a measure of the energy density, i.e., they indicate which states are populated by particles and have distinct manifestations for Majorana versus Dirac character. Conversely, particle-beam experiments measure cross sections and have difficulties discerning between the two characters as discussed in Refs. [94,95]. We do not advocate for using one method over the other. Rather, both should be pursued as they complement one another in probing the nature of neutrino interactions.

ACKNOWLEDGMENTS

\The authors thank Volker Koch, Volodymyr Vovchenko, Nicole Vassh, George Fuller, James Kneller, Gail McLaughlin, and Amol Patwardhan for useful discussions. E. G. is supported in part by the Department of Energy Office of Nuclear Physics Award No. DE-FG02-02ER41216, and by the National Science Foundation Grant No. PHY-1430152 (Joint Institute for Nuclear Astrophysics Center for the Evolution of the Elements). A. B. B. is support in part by the National Science Foundation Grant No. PHY-2108339 at University of Wisconsin Madison. A. B. B. and E. G. acknowledge support in part by the National Science Foundation Grants No. PHY-1630782 and No. PHY-2020275 (Network for Neutrinos Astrophysics and Symmetries). This research used resources provided by the Los Alamos National Laboratory Institutional Computing Program, which is supported by the U.S. Department of Energy National Nuclear Security Administration under Contract No. 89233218CNA000001.

APPENDIX A: DIFFERENTIAL CROSS SECTIONS WITH A MAGNETIC MOMENT VERTEX

Here we give differential cross sections for the various scattering and annihilation processes with fermions and bosons. The differential cross sections are functions of Mandelstam variable $t = (p_1 - p_3)^2$ for the reaction $1 + 2 \leftrightarrow 3 + 4$, and depend on Mandelstam variable $s = (p_1 + p_2)^2$, the neutrino magnetic moment strength μ, the effective in-medium photon mass m_γ from Eq. (3), and the vacuum mass of the charged boson/fermion. We calculate the integrated cross sections using

$$\sigma(s) = \int_{t_{\rm min}}^{t_{\rm max}} dt \frac{d\sigma}{dt}, \tag{A1}$$

where the limits of integration are

$$t_{\rm min} = -\frac{(s - m_i^2)^2}{s}, \tag{A2}$$

$$t_{\rm max} = 0. \tag{A3}$$

1. Fermions

Equation (5) gave the differential cross section for the scattering of neutrinos from charged fermions of mass m_f and charge coefficient q_f

$$\left(\frac{d\sigma}{dt}\right)_{\nu f} = \frac{\pi q_f^2 \alpha^2}{m_e^2}\mu^2 \frac{t}{(t - m_\gamma^2)^2}\frac{s + t - m_f^2}{s - m_f^2}. \tag{A4}$$

Figure 11 shows a contour plot of the total cross section in the m_γ versus s plane. The magnetic moment contribution to the neutrino-antineutrino annihilation differential cross section into charged fermion-antifermion pairs each with mass m_f is given by

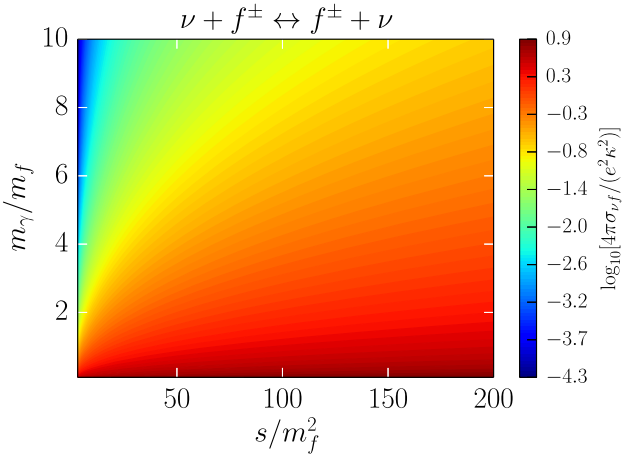

FIG. 11. m_γ versus kinetic variable s plotted at contours of constant $\sigma_{\nu f}$ for $\nu + f^{\pm} \leftrightarrow f^{\pm} + \nu$ elastic scattering channel [see Eq. (A4)]. We take $q_f = 1$ in this figure.

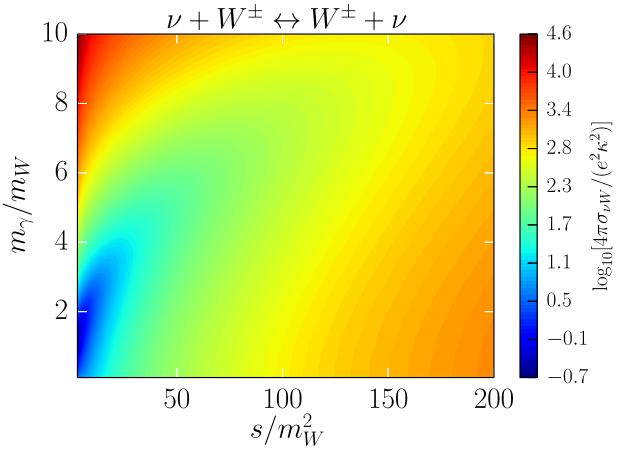

FIG. 12. m_γ versus kinetic variable s plotted at contours of constant $\sigma_{\nu W}$ for $\nu + W^{\pm} \leftrightarrow W^{\pm} + \nu$ elastic scattering channel [see Eq. (A6)].

$$\left(\frac{d\sigma}{dt}\right)_{f\bar{f}} = \left(\frac{2\pi q_f^2 \alpha^2}{m_e^2}\right)\mu^2 \frac{1}{s(s-m_\gamma^2)^2}(t + s - m_f^2)(m_f^2 - t). \tag{A5}$$

2. Bosons

The only boson particle we consider is $W^{\pm}$. The cross section for the magnetic moment contribution to the scattering of neutrinos from W bosons with mass $m_W \simeq 80.4$ GeV is given by

$$\left(\frac{d\sigma}{dt}\right)_{\nu W} = \frac{\pi\alpha^2}{m_e^2}\mu^2 \frac{t}{(t-m_\gamma^2)^2}\left[\left(1 - \frac{t}{3m_W^2} + \frac{t^2}{4m_W^4}\right)\frac{s + t - m_W^2}{s - m_W^2} + \left(-\frac{5}{12} - \frac{t}{16m_W^2} + \frac{t^2}{16m_W^4}\right)\frac{t^2}{(s-m_W^2)^2}\right]. \tag{A6}$$

Figure 12 gives contours of total cross section in the m_γ versus s plane. Finally, the magnetic moment contribution to the neutrino-antineutrino annihilation cross section into $W^+ - W^-$ pairs is given by

$$\left(\frac{d\sigma}{dt}\right)_{W^+W^-} = \frac{e^2\kappa^2}{16\pi}\frac{1}{s(s-m_\gamma^2)^2}\left[(s + 2t - m_W^2)^2\left(3 - \frac{s}{m_W^2} + \frac{s^2}{4m_W^4}\right) + 8s\left(-s + \frac{s^2}{4m_W^2}\right)\right]. \tag{A7}$$

In calculating the cross sections involving W bosons we ignored the four-boson couplings since the associated amplitudes are suppressed by another order of the magnetic moment.

3. Hadrons

The cross section for scattering on scalar charged hadrons with mass m_h is

$$\left(\frac{d\sigma}{dt}\right)_{\nu h} = \frac{e^2\kappa^2}{4\pi}\frac{t}{(t-m_\gamma^2)^2}\left[1 + \frac{t}{s-m_h^2} + \frac{t^2}{4(s-m_h^2)^2}\right]. \tag{A8}$$

Figure 13 gives contours of total cross section in the m_γ versus m_h plane. We take the annihilation cross section into scalar hadron-antihardron pairs to be zero. In the case of charged vector hadrons, we ignore the contributions to the scattering rates, and so do not provide the scattering and annihilation differential cross sections. Although these rates would be nonzero, we estimate only a small error as the vector hadrons have large masses and do not appear in appreciable numbers at temperatures below the QHT (see rows 7 and 9 in Table II).

APPENDIX B: THERMALLY AVERAGED CROSS SECTIONS

1. Elastic scattering

We use the thermally averaged product of σ and $v_{\rm Mol}$, denoted $\langle\sigma v_{\rm Mol}\rangle$, to calculate scattering rates between neutrinos and other particles via the magnetic-moment vertex. The formula for the thermal average is the following:

$$\langle \sigma v_{\rm Mol} \rangle = \frac{\frac{g_1 g_2}{(2\pi)^6} \int d^3p_1 \frac{1}{e^{E_1/T}+1} \int d^3p_2 \sigma v_{\rm Mol} \frac{1}{e^{E_2/T}\pm 1}}{\frac{g_1 g_2}{(2\pi)^6} \int d^3p_1 \frac{1}{e^{E_1/T}+1} \int d^3p_2 \frac{1}{e^{E_2/T}\pm 1}}, \tag{B1}$$

$$= \frac{g_1 g_2}{(2\pi)^6 n_1 n_2} \int d^3p_1 \frac{1}{e^{E_1/T}+1} \times \int d^3p_2 \sigma v_{\rm Mol} \frac{1}{e^{E_2/T}\pm 1}, \tag{B2}$$

where we have assumed equilibrium distributions and ignored the Pauli blocking/Bose enhancement of the products. Particle 1 is the neutrino with zero rest mass, and particle 2 is the scattering target with rest mass m. The ± 1 in the distribution function for the second particle corresponds to either fermions (+) or bosons (−). Both σ and $v_{\rm Mol}$ are given in terms of Mandelstam variable s, particle 2 mass m, and the in-medium photon mass m_γ.

With a change in variables and using $v_{\rm Mol} = (s-m^2)/2E_1E_2$ [61], we can reduce the expression in Eq. (B2) to a double integral. For fermions, that expression is

$$\langle \sigma v_{\rm Mol} \rangle_{\rm FD} = \frac{2g_1 g_2 \pi^2 T^6}{(2\pi)^6 n_1 n_2} \int_{\epsilon_m^2}^{\infty} d\epsilon_s (\epsilon_s - \epsilon_m^2)\sigma \int_{\sqrt{\epsilon_s}}^{\infty} d\epsilon_+ \frac{1}{e^{\epsilon_+}-1} \times \left\{ \beta + \ln\left[\frac{1 + 2e^{(-\beta-\epsilon_+)/2}\cosh(\frac{\alpha}{2}) + e^{-\beta-\epsilon_+}}{1 + 2e^{(\beta-\epsilon_+)/2}\cosh(\frac{\alpha}{2}) + e^{\beta-\epsilon_+}} \right] \right\}, \tag{B3}$$

where the ϵ notation denotes an energy quantity normalized by the appropriate power of T, namely $\epsilon_s = s/T^2$, $\epsilon_+ = E_+/T$, $\epsilon_m = m/T$, and $\epsilon_\gamma = m_\gamma/T$. We rewrite σ as a function of ϵ_s, ϵ_m, ϵ_γ, and T. In Eq. (B3), we have also defined new quantities for ease in writing

$$\alpha = \epsilon_+ \frac{\epsilon_m^2}{\epsilon_s}, \qquad \beta = \frac{\epsilon_s - \epsilon_m^2}{\epsilon_s}\sqrt{\epsilon_+^2 - \epsilon_s}. \tag{B4}$$

Our expression in Eq. (B3) is the same as Eq. (B6) in Ref. [25] where we have corrected a few typographical errors.

For bosons, the thermal average for elastic scattering is

$$\langle \sigma v_{\rm Mol} \rangle_{\rm BE} = \frac{2g_1 g_2 \pi^2 T^6}{(2\pi)^6 n_1 n_2} \int_{\epsilon_m^2}^{\infty} d\epsilon_s (\epsilon_s - \epsilon_m^2)\sigma \int_{\sqrt{\epsilon_s}}^{\infty} d\epsilon_+ \frac{1}{e^{\epsilon_+}+1} \times \ln\left[\frac{\sinh(\frac{\alpha}{2}) + \sinh(\frac{\epsilon_+ + \beta}{2})}{\sinh(\frac{\alpha}{2}) + \sinh(\frac{\epsilon_+ - \beta}{2})} \right], \tag{B5}$$

with the same notation as Eq. (B3).

2. Annihilation scattering

For the annihilation channels, the expression for $\langle \sigma v_{\rm Mol} \rangle$ is the same for either boson or fermion pairs with mass m, as we average over the initial neutrino-antineutrino distributions. The result is the same expression as Eq. (B3) except with a different threshold value of s and massless reactants

$$\langle \sigma v_{\rm Mol} \rangle_{\rm ann} = \frac{4g_1 g_2 \pi^2 T^6}{(2\pi)^6 n_1 n_2} \int_{4\epsilon_m^2}^{\infty} d\epsilon_s \epsilon_s \sigma \int_{\sqrt{\epsilon_s}}^{\infty} d\epsilon_+ \frac{1}{e^{\epsilon_+}-1} \times \ln\left[\frac{\cosh(\frac{\epsilon_+ + \beta}{4})}{\cosh(\frac{\epsilon_+ - \beta}{4})} \right], \tag{B6}$$

where $\beta = \sqrt{\epsilon_+^2 - \epsilon_s}$.

APPENDIX C: TREATMENT OF QUARK-HADRON TRANSITION IN THE EARLY UNIVERSE

We have considered a range of models of anomalous magnetic moments which include decoupling of the inactive Dirac states in the $T \sim 100$ MeV range. Decoupling in this range is complicated by the transition from free quarks and gluons to bound hadrons in an expanding and cooling Universe. As a result, we model this epoch using a smooth crossover from a quark-gluon equation of state to one dominated by hadrons.

At high temperatures, we approximate the quark-gluon (qg) component as an ideal gas with negligible chemical potential. The qg component includes the six quark and gluon degrees of freedom with appropriate degeneracy factors. Conversely, at low temperature, we also approximate the hadron (h) component as an ideal gas with negligible chemical potential. We use the lightest hadrons shown in Table II. The next heaviest hadrons after the $K^{*0}(896)$ states are protons and neutrons. We have verified that excluding those baryons from the hadron component do not alter any of our results.

We use the combination of qg and h components to calculate thermodynamic quantities and the Debye

TABLE II. Table of hadrons used in the early Universe for this work. First column is name/symbol of the particle. Second, third, and fourth columns are mass (MeV), charge, and degeneracy (respectively). All positively charged hadrons have negatively charged partners. All particles are bosons.

Name	Mass (MeV)	Charge	Degeneracy
π^0	135.0	0	1
π^+	140.0	1	1
K^+	494.0	1	1
K^0	498.0	0	2
η^0	548.0	0	1
ρ^0	775.0	0	3
ρ^+	775.0	1	3
ω^0	783.0	0	3
$K^{*+}(892)$	892.0	1	3
$K^{*0}(896)$	896.0	0	6

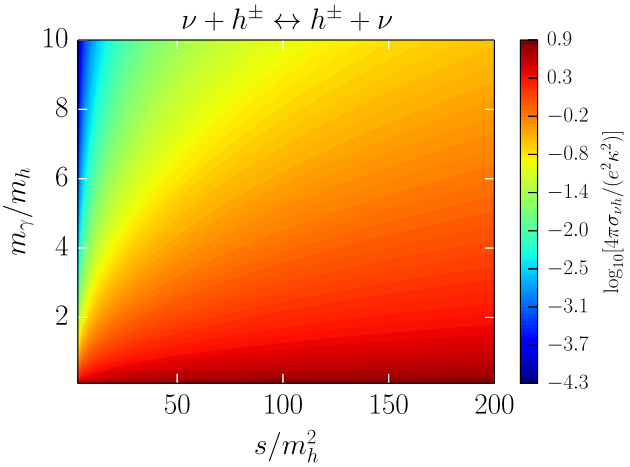

FIG. 13. m_γ versus kinetic variable s plotted at contours of constant $\sigma_{\nu h}$ for $\nu + h^{\pm} \leftrightarrow h^{\pm} + \nu$ elastic scattering channel [see Eq. (A8)].

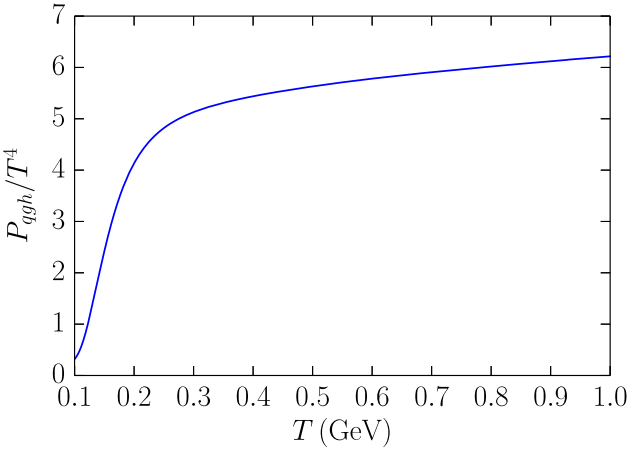

FIG. 14. Pressure of quark-hadron components versus temperature [see Eq. (C3)]. At high temperature, the system approaches that of an ideal gas of quarks and gluons. At low temperature, the system approaches that of an ideal gas of hadrons. For temperatures in the 100 MeV range, results are used from lattice QCD.

screening length. We denote the pressure, entropic density, number density, and energy density for the qg component as P_{qg}, s_{qg}, n_{qg}, and ρ_{qg}, respectively. For the hadrons, we replace the qg subscript with an h. To weight the contributions from the two seas when both components are present, we use a switching function following a prescription from Ref. [27]

$$S(T,\mu) = \exp[-\theta(T,\mu)], \tag{C1}$$

$$\theta(T,\mu) = \left[\left(\frac{T}{T_0}\right)^r + \left(\frac{\mu}{\mu_0}\right)^r\right]^{-1}. \tag{C2}$$

The switching function uses data calculated with lattice QCD [96] to fit the parameters T_0, μ_0, and r. We use $r = 4$, $T_0 = 145.33$ MeV, and $\mu_0 = 3\pi T_0$ from the first row of Table I in Ref. [27]. μ is the chemical potential.

According to the procedure in Ref. [27], we apply the switching function directly to the pressure

$$P_{qgh} = S(T,\mu)P_{qg} + [1 - S(T,\mu)]P_h, \tag{C3}$$

where P_{qgh} is the total pressure supplied by the quarks, gluons, and hadrons. Figure 14 shows P_{qgh}/T^4 as a function of T for $\mu = 0$. The increase in P_{qgh} between $T = 100$ MeV and $T = 200$ MeV is due to the appearance of the qg degrees of freedom and concomitant disappearance of the h degrees of freedom. The expressions for s, n, and ρ follow from derivatives of the pressure

$$s_{qgh} = Ss_{qg} + (1-S)s_h + S\frac{r\theta^2}{T}\left(\frac{T}{T_0}\right)^r (P_{qg} - P_h), \tag{C4}$$

$$n_{qgh} = Sn_{qg} + (1-S)n_h + S\frac{r\theta^2}{\mu}\left(\frac{\mu}{\mu_0}\right)^r (P_{qg} - P_h), \tag{C5}$$

$$\rho_{qgh} = Ts_{qgh} - P_{qgh} + \mu n_{qgh}. \tag{C6}$$

When calculating the inverse square of the Debye length in Eq. (2), the relevant quantity is the derivative of the number density with respect to μ. We would need to take the derivative of Eq. (C5) with respect to μ to calculate m_γ^2 during the QHT with the switching function. However, in the CP-symmetric conditions of the early Universe, all derivatives of the switching function with respect to μ are zero for $\mu = 0$. Hence, the expression for the contribution to m_γ^2 from the quark-gluon-hadron components are

$$m_{\gamma,qgh}^2 = 4\pi\alpha\left\{S(T,\mu=0)\sum_j q_j^2 \frac{\partial}{\partial\mu}\left[n_j^{(-)} - n_j^{(+)}\right] + [1 - S(T,\mu=0)]\sum_k q_k^2 \frac{\partial}{\partial\mu}\left[n_k^{(-)} - n_k^{(+)}\right]\right\}, \tag{C7}$$

where the first summation is over quark pairs and the second summation is over charged hadron pairs.

[1] L. Brown, The idea of the neutrino, Phys. Today **31**, 9, 23 (1978).

[2] Jeremy Bernstein, Malvin Ruderman, and Gerald Feinberg, Electromagnetic Properties of the neutrino, Phys. Rev. **132**, 1227 (1963).

[3] John A Morgan, Anomalous neutrino interactions and primordial nucleosynthesis, Mon. Not. R. Astron. Soc. **195**, 173 (1981).

[4] J. A. Morgan, Cosmological upper limit to neutrino magnetic moments, Phys. Lett. **102B**, 247 (1981).

[5] L. B. Okun, M. B. Voloshin, and M. I. Vysotsky, Electromagnetic properties of neutrino and possible semiannual variation cycle of the solar neutrino flux, Sov. J. Nucl. Phys. **44**, 440 (1986).

[6] L. B. Okun, M. B. Voloshin, and M. I. Vysotsky, Neutrino electrodynamics and possible effects for solar neutrinos, Sov. Phys. JETP **64**, 446 (1986).

[7] Georg G. Raffelt, Core mass at the helium flash from observations and a new bound on neutrino electromagnetic properties, Astrophys. J. **365**, 559 (1990).

[8] Chong-Sa Lim and William J. Marciano, Resonant spin-flavor precession of solar and supernova neutrinos, Phys. Rev. D **37**, 1368 (1988).

[9] Evgeny K. Akhmedov, Resonant amplification of neutrino spin rotation in matter and the solar neutrino problem, Phys. Lett. B **213**, 64 (1988).

[10] A. B. Balantekin, P. J. Hatchell, and F. Loreti, Matter enhanced spin flavor precession of solar neutrinos with transition magnetic moments, Phys. Rev. D **41**, 3583 (1990).

[11] A. D. Dolgov, Neutrinos in cosmology, Phys. Rep. **370**, 333 (2002).

[12] Arturo Cisneros, Effect of neutrino magnetic moment on solar neutrino observations, Astrophys. Space Sci. **10**, 87 (1971).

[13] J. Martín-Albo *et al.* (NEXT Collaboration), Sensitivity of NEXT-100 to neutrinoless double beta decay, J. High Energy Phys. 05 (2016) 159.

[14] J. B. Albert *et al.* (EXO Collaboration), Search for Neutrinoless Double-Beta Decay with the Upgraded EXO-200 Detector, Phys. Rev. Lett. **120**, 072701 (2018).

[15] D. Q. Adams *et al.* (CUORE Collaboration), Improved Limit on Neutrinoless Double-Beta Decay in ^{130}Te with CUORE, Phys. Rev. Lett. **124**, 122501 (2020).

[16] M. Agostini *et al.* (GERDA Collaboration), Final Results of GERDA on the Search for Neutrinoless Double-β Decay, Phys. Rev. Lett. **125**, 252502 (2020).

[17] N. Abgrall *et al.* (LEGEND Collaboration), The large enriched Germanium experiment for neutrinoless $\beta\beta$ decay: LEGEND-1000 Preconceptual Design Report, arXiv:2107.11462.

[18] V. Albanese *et al.* (SNO + Collaboration), The SNO + experiment, J. Instrum. **16**, P08059 (2021).

[19] S. Abe *et al.* (KamLAND-Zen Collaboration), Search for the Majorana Nature of Neutrinos in the Inverted Mass Ordering Region with KamLAND-Zen, Phys. Rev. Lett. **130**, 051801 (2023).

[20] I. J. Arnquist *et al.* (Majorana Collaboration), Final Result of the Majorana Demonstrator's Search for Neutrinoless Double-β Decay in Ge76, Phys. Rev. Lett. **130**, 062501 (2023).

[21] G. Steigman, D. N. Schramm, and J. E. Gunn, Cosmological limits to the number of massive leptons, Phys. Lett. **66B**, 202 (1977).

[22] J. E. Gunn, B. W. Lee, I. Lerche, D. N. Schramm, and G. Steigman, Some astrophysical consequences of the existence of a heavy stable neutral lepton, Astrophys. J. **223**, 1015 (1978).

[23] Martina Gerbino *et al.*, Synergy between cosmological and laboratory searches in neutrino physics, arXiv:2203.07377.

[24] M. Fukugita and S. Yazaki, Reexamination of astrophysical and cosmological constraints on the magnetic moment of neutrinos, Phys. Rev. D **36**, 3817 (1987).

[25] N. Vassh, E. Grohs, A. B. Balantekin, and G. M. Fuller, Majorana neutrino magnetic moment and neutrino decoupling in big bang nucleosynthesis, Phys. Rev. D **92**, 125020 (2015).

[26] M. S. Dvornikov and A. I. Studenikin, Electromagnetic form factors of a massive neutrino, Sov. J. Exp. Theor. Phys. **99**, 254 (2004).

[27] M. Albright, J. Kapusta, and C. Young, Matching excluded-volume hadron-resonance gas models and perturbative QCD to lattice calculations, Phys. Rev. C **90**, 024915 (2014).

[28] C. Broggini, C. Giunti, and A. Studenikin, Electromagnetic properties of neutrinos, Adv. High Energy Phys. **2012**, 459526 (2012).

[29] Carlo Giunti and Alexander Studenikin, Neutrino electromagnetic interactions: A window to new physics, Rev. Mod. Phys. **87**, 531 (2015).

[30] A. Baha Balantekin and Boris Kayser, On the properties of neutrinos, Annu. Rev. Nucl. Part. Sci. **68**, 313 (2018).

[31] Benjamin W. Lee and Robert E. Shrock, Natural suppression of symmetry violation in gauge theories: Muon—lepton and electron lepton number nonconservation, Phys. Rev. D **16**, 1444 (1977).

[32] Kazuo Fujikawa and Robert Shrock, The Magnetic Moment of a Massive Neutrino and Neutrino Spin Rotation, Phys. Rev. Lett. **45**, 963 (1980).

[33] A. B. Balantekin and N. Vassh, Magnetic moments of active and sterile neutrinos, Phys. Rev. D **89**, 073013 (2014).

[34] A. G. Beda, V. B. Brudanin, V. G. Egorov, D. V. Medvedev, V. S. Pogosov, M. V. Shirchenko, and A. S. Starostin, The results of search for the neutrino magnetic moment in GEMMA experiment, Adv. High Energy Phys. **2012**, 350150 (2012).

[35] E. Aprile *et al.* (XENON Collaboration), Excess electronic recoil events in XENON1T, Phys. Rev. D **102**, 072004 (2020).

[36] O. G. Miranda, D. K. Papoulias, M. Tórtola, and J. W. F. Valle, XENON1T signal from transition neutrino magnetic moments, Phys. Lett. B **808**, 135685 (2020).

[37] Xiaopeng Zhou *et al.* (PandaX-II Collaboration), A search for solar axions and anomalous neutrino magnetic moment with the complete PandaX-II data, Chin. Phys. Lett. **38**, 011301 (2021); **38**, 109902(E) (2021).

[38] M. Atzori Corona, W. M. Bonivento, M. Cadeddu, N. Cargioli, and F. Dordei, New constraint on neutrino magnetic moment and neutrino millicharge from LUX-ZEPLIN

dark matter search results, Phys. Rev. D **107**, 053001 (2023).
[39] ShivaSankar K. A., Anirban Majumdar, Dimitrios K. Papoulias, Hemant Prajapati, and Rahul Srivastava, Implications of first LZ and XENONnT results: A comparative study of neutrino properties and light mediators, Phys. Lett. B **839**, 137742 (2023).
[40] J. M. Lattimer and J. Cooperstein, Limits on the Neutrino Magnetic Moment from SN 1987a, Phys. Rev. Lett. **61**, 23 (1988); **61**, 2633(E) (1988).
[41] Riccardo Barbieri and Rabindra N. Mohapatra, Limit on the Magnetic Moment of the Neutrino from Supernova SN 1987a Observations, Phys. Rev. Lett. **61**, 27 (1988).
[42] Dirk Notzold, New bounds on neutrino magnetic moments From stellar collapse, Phys. Rev. D **38**, 1658 (1988).
[43] Francesco Capozzi and Georg Raffelt, Axion and neutrino bounds improved with new calibrations of the tip of the red-giant branch using geometric distance determinations, Phys. Rev. D **102**, 083007 (2020).
[44] Kanji Mori, A. Baha Balantekin, Toshitaka Kajino, and Michael A. Famiano, Elimination of the blue loops in the evolution of intermediate-mass stars by the neutrino magnetic moment and large extra dimensions, Astrophys. J. **901**, 115 (2020).
[45] Kanji Mori, Motohiko Kusakabe, A. Baha Balantekin, Toshitaka Kajino, and Michael A. Famiano, Enhancement of lithium in red clump stars by the additional energy loss induced by new physics, Mon. Not. R. Astron. Soc. **503**, 2746 (2021).
[46] Alejandro H. Córsico, Leandro G. Althaus, Marcelo M. Miller Bertolami, S. O. Kepler, and Enrique García-Berro, Constraining the neutrino magnetic dipole moment from white dwarf pulsations, J. Cosmol. Astropart. Phys. 08 (2014) 054.
[47] Marcelo Miguel Miller Bertolami, Limits on the neutrino magnetic dipole moment from the luminosity function of hot white dwarfs, Astron. Astrophys. **562**, A123 (2014).
[48] K. S. Babu, Sudip Jana, and Manfred Lindner, Large neutrino magnetic moments in the light of recent experiments, J. High Energy Phys. 10 (2020) 040.
[49] Shao-Feng Ge and Stephen J. Parke, Scalar Nonstandard Interactions in Neutrino Oscillation, Phys. Rev. Lett. **122**, 211801 (2019).
[50] Alexei Yu Smirnov and Xun-Jie Xu, Wolfenstein potentials for neutrinos induced by ultra-light mediators, J. High Energy Phys. 12 (2019) 046.
[51] K. S. Babu, Garv Chauhan, and P. S. Bhupal Dev, Neutrino nonstandard interactions via light scalars in the Earth, Sun, supernovae, and the early Universe, Phys. Rev. D **101**, 095029 (2020).
[52] Ashutosh Kumar Alok, Neetu Raj Singh Chundawat, and Arindam Mandal, Cosmic neutrino flux and spin flavor oscillations in intergalactic medium, Phys. Lett. B **839**, 137791 (2023).
[53] Vedran Brdar, Admir Greljo, Joachim Kopp, and Toby Opferkuch, The neutrino magnetic moment portal: Cosmology, astrophysics, and direct detection, J. Cosmol. Astropart. Phys. 01 (2021) 039.
[54] O. G. Miranda, D. K. Papoulias, O. Sanders, M. Tórtola, and J. W. F. Valle, Low-energy probes of sterile neutrino transition magnetic moments, J. High Energy Phys. 12 (2021) 191.
[55] Vedran Brdar, André de Gouvêa, Ying-Ying Li, and Pedro A. N. Machado, Neutrino magnetic moment portal and supernovae: New constraints and multimessenger opportunities, Phys. Rev. D **107**, 073005 (2023).
[56] Per Elmfors, Kari Enqvist, Georg Raffelt, and Günter Sigl, Neutrinos with magnetic moment: Depolarization rate in plasma, Nucl. Phys. **B503**, 3 (1997).
[57] A. Ayala, J. C. D'Olivo, and M. Torres, Right-handed neutrino production in dense and hot plasmas, Nucl. Phys. **B1**, 204 (2000).
[58] Pierluca Carenza, Giuseppe Lucente, Martina Gerbino, Maurizio Giannotti, and Massimiliano Lattanzi, Strong cosmological constraints on the neutrino magnetic moment, arXiv:2211.10432.
[59] Shao-Ping Li and Xun-Jie Xu, Neutrino magnetic moments meet precision N_{eff} measurements, J. High Energy Phys. 02 (2023) 085.
[60] Eunseok Hwang, Dukjae Jang, Kiwan Park, Motohiko Kusakabe, Toshitaka Kajino, A. Baha Balantekin, Tomoyuki Maruyama, Chang-Mo Ryu, and Myung-Ki Cheoun, Dynamical screening effects on big bang nucleosynthesis, J. Cosmol. Astropart. Phys. 11 (2021) 017.
[61] P. Gondolo and G. Gelmini, Cosmic abundances of stable particles: Improved analysis, Nucl. Phys. **B360**, 145 (1991).
[62] E. W. Kolb and M. S. Turner, *The Early Universe* (Addison-Wesley Publishing Co., Reading, MA, 1990).
[63] Michael J. Ramsey-Musolf, The electroweak phase transition: A collider target, J. High Energy Phys. 09 (2020) 179.
[64] A. D. Dolgov, S. H. Hansen, and D. V. Semikoz, Non-equilibrium corrections to the spectra of massless neutrinos in the early universe, Nucl. Phys. **B503**, 426 (1997).
[65] G. Mangano, G. Miele, S. Pastor, and M. Peloso, A precision calculation of the effective number of cosmological neutrinos, Phys. Lett. B **534**, 8 (2002).
[66] Jeremiah Birrell, Cheng Tao Yang, and Johann Rafelski, Relic neutrino freeze-out: Dependence on natural constants, Nucl. Phys. **B890**, 481 (2015).
[67] E. Grohs, G. M. Fuller, C. T. Kishimoto, M. W. Paris, and A. Vlasenko, Neutrino energy transport in weak decoupling and big bang nucleosynthesis, Phys. Rev. D **93**, 083522 (2016).
[68] Cyril Pitrou, Alain Coc, Jean-Philippe Uzan, and Elisabeth Vangioni, Precision big bang nucleosynthesis with improved Helium-4 predictions, Phys. Rep. **754**, 1 (2018).
[69] Miguel Escudero Abenza, Precision early universe thermodynamics made simple: N_{eff} and neutrino decoupling in the Standard Model and beyond, J. Cosmol. Astropart. Phys. 05 (2020) 048.
[70] Kensuke Akita and Masahide Yamaguchi, A precision calculation of relic neutrino decoupling, J. Cosmol. Astropart. Phys. 08 (2020) 012.
[71] Julien Froustey, Cyril Pitrou, and Maria Cristina Volpe, Neutrino decoupling including flavour oscillations and primordial nucleosynthesis, J. Cosmol. Astropart. Phys. 12 (2020) 015.
[72] Jack J. Bennett, Gilles Buldgen, Pablo F. De Salas, Marco Drewes, Stefano Gariazzo, Sergio Pastor, and Yvonne Y. Y. Wong, Towards a precision calculation of N_{eff} in the

Standard Model II: Neutrino decoupling in the presence of flavour oscillations and finite-temperature QED, J. Cosmol. Astropart. Phys. 04 (2021) 073.
[73] Planck Collaboration, Planck 2018 results. VI. Cosmological parameters, Astron. Astrophys. **641**, A6 (2020).
[74] J. E. Carlstrom *et al.* (CMB-S4 Collaboration), CMB-S4 Science Book, First Edition, arXiv:1610.02743.
[75] Evan Grohs and George M. Fuller, Big bang nucleosynthesis, arXiv:2301.12299.
[76] Richard H. Cyburt, Brian D. Fields, Keith A. Olive, and Tsung-Han Yeh, Big bang nucleosynthesis: Present status, Rev. Mod. Phys. **88**, 015004 (2016).
[77] James P. Kneller and Gary Steigman, BBN for pedestrians, New J. Phys. **6**, 117 (2004).
[78] Julien Lesgourgues and Sergio Pastor, Massive neutrinos and cosmology, Phys. Rep. **429**, 307 (2006).
[79] Yvonne Y. Y. Wong, Neutrino mass in cosmology: Status and prospects, Annu. Rev. Nucl. Part. Sci. **61**, 69 (2011).
[80] Cora Dvorkin, Martina Gerbino, David Alonso, Nicholas Battaglia, Simeon Bird, Ana Diaz Rivero, Andreu Font-Ribera, George Fuller, Massimiliano Lattanzi, Marilena Loverde, Julian B. Muñoz, Blake Sherwin, Anze Slosar, and Francisco Villaescusa-Navarro, Neutrino mass from cosmology: Probing physics beyond the standard model, Bull. Am. Astron. Soc. **51**, 64 (2019).
[81] P. A. Zyla *et al.* (Particle Data Group), Review of particle physics, Prog. Theor. Exp. Phys. **2020**, 083C01 (2020), and 2021 update.
[82] R. C. Allen, H. H. Chen, P. J. Doe, R. Hausammann, W. P. Lee, X. Q. Lu, H. J. Mahler, M. E. Potter, K. C. Wang, T. J. Bowles, R. L. Burman, R. D. Carlini, D. R. Cochran, J. S. Frank, E. Piasetzky, V. D. Sandberg, D. A. Krakauer, and R. L. Talaga, Study of electron-neutrino-electron elastic scattering at LAMPF, Phys. Rev. D **47**, 11 (1993).
[83] L. B. Auerbach *et al.*, Measurement of electron-neutrino electron elastic scattering, Phys. Rev. D **63**, 112001 (2001).
[84] R. Schwienhorst *et al.* (DONUT Collaboration), A new upper limit for the tau-neutrino magnetic moment, Phys. Lett. B **513**, 23 (2001).
[85] C. Arpesella *et al.* (Borexino Collaboration), Direct Measurement of the Be-7 Solar Neutrino Flux with 192 Days of Borexino Data, Phys. Rev. Lett. **101**, 091302 (2008).
[86] Carlo Giunti and Alexander Studenikin, Neutrino electromagnetic interactions: A window to new physics, Rev. Mod. Phys. **87**, 531 (2015).
[87] Peter Adshead, Yanou Cui, Andrew J. Long, and Michael Shamma, Unraveling the Dirac neutrino with cosmological and terrestrial detectors, Phys. Lett. B **823**, 136736 (2021).
[88] Rabindra N. Mohapatra and Goran Senjanović, Neutrino Mass and Spontaneous Parity Nonconservation, Phys. Rev. Lett. **44**, 912 (1980).
[89] André de Gouvêa, Ivan Martinez-Soler, Yuber F. Perez-Gonzalez, and Manibrata Sen, Fundamental physics with the diffuse supernova background neutrinos, Phys. Rev. D **102**, 123012 (2020).
[90] André de Gouvêa, Wei-Chih Huang, and James Jenkins, Pseudo-Dirac neutrinos in the new standard model, Phys. Rev. D **80**, 073007 (2009).
[91] John Beacom, Nicole Bell, and Scott Dodelson, Neutrinoless Universe, Phys. Rev. Lett. **93**, 121302 (2004).
[92] Pasquale Serpico, Cosmological Neutrino Mass Detection: The Best Probe of Neutrino Lifetime, Phys. Rev. Lett. **98**, 171301 (2007).
[93] Yasaman Farzan and Steen Hannestad, Neutrinos secretly converting to lighter particles to please both KATRIN and the cosmos, J. Cosmol. Astropart. Phys. 02 (2016) 058.
[94] Boris Kayser, Majorana neutrinos and their electromagnetic properties, Phys. Rev. D **26**, 1662 (1982).
[95] Boris Kayser and Robert E. Shrock, Distinguishing between Dirac and Majorana neutrinos in neutral current reactions, Phys. Lett. **112B**, 137 (1982).
[96] Szabolcs Borsanyi, Gergely Endrodi, Zoltan Fodor, Antal Jakovac, Sandor D. Katz, Stefan Krieg, Claudia Ratti, and Kalman K. Szabo, The QCD equation of state with dynamical quarks, J. High Energy Phys. 11 (2010) 077.